A Numerical Study of ZNMF Jet Lift Enhancement of a NACA 0015 Airfoil

Vassili KITSIOS, Andrew OOI

Walter Basset Aerodynamics Laboratory, The University of Melbourne, VIC, 3010

Julio SORIA

Laboratory for Turbulence Research in Aerospace and Combustion, Monash University, Clayton, VIC, 3800

Donghyun YOU

Center for Turbulence Research, Stanford University, CA, 94305

Abstract. This paper reports on a numerical study that investigates how the boundary layer properties of an airfoil are modified with the implementation of aerodynamic control via zero-net-mass-flux (ZNMF) jets. Highlighted are the means by which separation can be modified and controlled to achieve lift enhancement. The flow configuration is a NACA 0015 airfoil with a ZNMF jet normal to the surface, spanning the entire leading edge. Complementary water tunnel experiments of this flow configuration are detailed in [12]. Integrated lift and drag measurements were taken for a range of angles of attack (α). Flow visualisations and quantitative PIV measurements of the velocity field were also taken at $\alpha = 18°$, where the largest lift enhancement was observed. A three-dimensional (3-D) Large-Eddy Simulation (LES) of the uncontrolled case at $\alpha = 18°$ is conducted and agrees well with both the force measurements and PIV data, while 3-D LES simulations of the controlled case are ongoing. In order to study the effects of the forcing frequencies on the flow field, 2-D simulations were carried out to identify how the attached boundary layer properties change over a range of forcing frequencies. For all forcing frequencies, the ZNMF jet decreases the boundary layer momentum thickness, indicating a steeper velocity profile that delayed the onset of separation. However, the control frequencies that best minimise separation determined by the numerical calculations, differ from those identified in the experiments. Possible explanations for this discrepancy are discussed.

Key words: flow control, LES, wings, incompressible flow, instability.

1. Introduction

There are many approaches to flow control, the fundamental distinction being whether a particular approach is active or passive. Passive methods do not expend any energy, and the flowfield is modified through stationary geometric devices. Active control does adopts energetic forcing. Suction and blowing is the selected means of applying the active control in this particular study. Possibly the first instance of this form of active control was undertaken by Prandtl in 1904, who applied a steady blowing jet to a circular cylinder to delay separation [7].

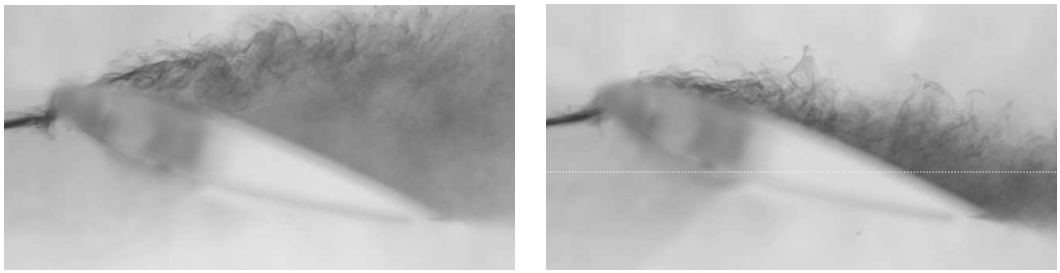

(a) (b)

Figure 1. Die streak flow visualisations of a NACA 0015 airfoil at $\alpha = 18°$. (a) uncontrolled; (b) controlled. Modified from [12]

The next level of complexity are oscillatory jets. With application to a NACA 0015 airfoil, at a Reynolds number based on chord length of $Re_c = 1 \times 10^6$, it has been shown that an oscillatory jet can achieve the same level of lift enhancement as a steady jet, but with an order of magnitude less energy [8]. A subset of oscillatory jets are ZNMF jets, as they are generated with zero net mass injection into the domain over one complete cycle. They are typically formed by an oscillating membrane within a cavity flush-mounted below the aerodynamic surface. The cavity locally inhales and exhales the working fluid, generating a non-zero momentum flow from its orifice. The result is a turbulent jet, that in the mean sense is qualitatively similar to a continuous jet [9]. In the case of circular orifices, the spreading rates and decay constants are larger compared to that of a continuous jet with equivalent Reynolds number based on the momentum velocity [1]. They therefore, have a more localised effect, leading to more precise control of the flowfield, and have been successfully applied to a range of flow configurations. A low-pressure turbine study illustrated jets normal to the wall were more effective than tangential blowing [11]. It has also been shown that on an airfoil at $Re_c = 3 \times 10^5$, jets closer to the uncontrolled separation point require a lower jet velocity to achieve the same lift enhancement [10].

Drawing from these previous findings, [12] later undertook experiments on a NACA 0015 airfoil at $Re_c = 3 \times 10^5$, with the ZNMF jet normal to the surface and spanning the entire leading edge. For angles of attack past the post-stall region, the ZNMF jet was near the uncontrolled separation point. The pertinent non-dimensional parameters in this system were $Re_c \equiv \frac{u_{ref} c}{\nu}$, non-dimensional forcing frequency $F^+ \equiv \frac{fc}{u_{ref}}$ and momentum blowing coefficient $c_\mu \equiv 2\frac{h}{c}(\frac{u_{j,rms}}{U_\infty})^2$, where f is the dimensional forcing frequency, h slot width and $u_{jet,rms}$ is the root mean square (rms) jet velocity. Force measurements were recorded for $0° < \alpha < 27°$, $0.3 < F^+ < 2$ and $c_\mu < 1.38 \times 10^{-3}$. The greatest lift enhancement was observed at $\alpha = 18°$ for $F^+ = 1.3$ and $c_\mu = 1.38 \times 10^{-3}$. Flow visualisations were then undertaken at $\alpha = 18°$ for the uncontrolled flow and the controlled flow with the parameters maximising lift enhancment. Dye streak visualisations gave a qualitative indication of the mean velocity fields, illustrating that the control significantly reduced the mean separated region (see Fig.1). Particle Image Velocimetry (PIV) measurements were also undertaken to quantify the velocity fields. The force measurements and PIV data are compared with the numerical simulations carried out in this study to validate the computational model.

The purpose of the present study is to numerically replicate the experimental study of [12] and compare to the available measurements. This work was initiated as part of the Stanford University Center for Turbulence Research (CTR) 2006 Summer Research Program and building upon the results published in [5]. As the velocity profiles were not measured in the experiments, this information will be extracted from the numerical models. The relationship between the boundary layer properties and forcing frequency of the ZNMF jet, will be investigated to gain further understanding of the mechanisms responsible for lift enhancement.

2. Computational Approach

2.1. Numerical model

The incompressible version of the code CDP is utilised to undertake the numerical simulations. CDP was developed at the Stanford CTR and is an unstructured finite volume based code [6]. 2-D simulations solving the incompressible Navier-Stokes equations without any turbulence models and 3-D LES are used in the present investigation. The dynamic Smagorinski subgrid scale (SGS) model of [2] is adopted for the 3-D LES calculations. Numerical dissipation is minimised by discretising the continuity and momentum equations such that they discretely conserve kinetic energy. This is enforced on the pressure and convective terms using the approach outlined in [6].

2.2. Flow configuration

A modified C-type grid of a NACA 0015 airfoil is adopted for all numerical simulations. The block topology is illustrated in Fig. 2(a). These grids are summarised by the inlet arc (C), the distance between the body and the outer boundary (N), and in the spanwise domain (Z). A Dirichlet boundary condition of $(u, v, w) = (u_{ref}, 0, 0)$ is applied at the inlet, top, and bottom boundaries. A Neumann boundary condition of $\frac{\partial u}{\partial x} = 0$ is applied at the outlet and a periodic boundary condition is applied in the spanwise direction. The computational domain is of size $L_C \times L_N \times L_Z = 28c \times 6c \times 1c$. The ZNMF jet cavity is modelled, with the slot normal to the surface spanning the entire leading edge. Consistent with the experiment, the slot is $1.5 \times 10^{-3}c$ wide and $3.0 \times 10^{-2}c$ long (see Fig. 2(c)). A Dirichlet boundary condition is used to prescribe the oscillatory velocity $u_{jet}(t) = \sqrt{2}u_{jet,rms}\sin(2\pi ft)$ at the bottom of the cavity.
The cell count is $N_C \times N_N \times N_Z = 808 \times 80 \times 20$, with 8 cells across the cavity slot. The cell spacing along the airfoil is $\Delta C/c = 1.875 \times 10^{-4}$ at the cavity and is stretched to a maximum size at the trailing edge of $\Delta C/c = 9.6 \times 10^{-3}$. The cell spacings are $\Delta N/c = 1.2 \times 10^{-3}$ and $\Delta Z/c = 5.0 \times 10^{-2}$, and in viscous units within the range of $\Delta C^+/c \leq 24$, $\Delta N^+/c \leq 3$, and $\Delta Z^+/c \leq 150$. The 2-D grids have the same properties, but with only 1 cell in the spanwise direction. The same grid was used for both the controlled and uncontrolled cases; in the latter the ZNMF boundary is treated as a slip wall.
The simulations are advanced in time with a constant time step size of $\frac{\Delta t u_{ref}}{c} = 4 \times 10^{-4}$. The maximum CFL number was approximately 3 in the grid partition containing the ZNMF jet, and less than unity in all other partitions. The characteristic fluid mechanical time scale is given by $t^\theta = \frac{\Theta_{BL}}{\tilde{u}_t}$, where Θ_{BL} is the boundary

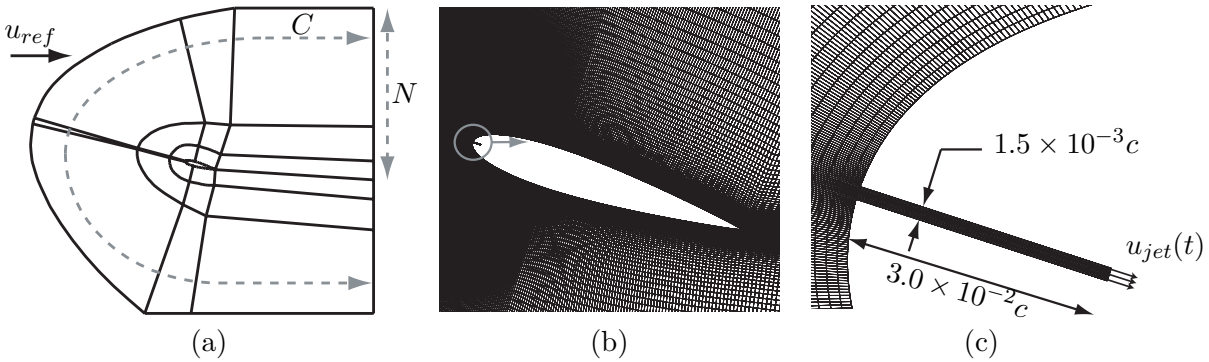

Figure 2. Topology of the modified C-type grid. (a) block topology; (b) body-fitted airfoil grid; (c) ZNMF jet cavity. [5]

layer momentum thickness immediately prior to separation, and $\hat{\overline{u}}_t$ is the maximum mean tangential velocity on the profile. It is calculated at the point of separation and found to be two orders of magnitude larger than the adopted time step, indicating that all temporal scales are resolved. All simulations presented are run until C_l reached a statistically stationary state and for a minimum period of $\frac{40c}{u_{ref}}$.

3. Results

The development of both the 2-D and 3-D numerical models for the parameters $Re = 3 \times 10^5$, $c_\mu = 1.38 \times 10^-3$, and $F^+ = 1.3$ are presented and compared to the experimental measurements to determine their validity. The forces from the experiments reported in this section were measured using a transducer with a resolution $0.1N$, which is equivalent to a lift coefficient resolution of $\Delta C_l = 0.042$. The forces were recorded over a period of approximately $\frac{300c}{u_{ref}}$, with temporal mean and standard deviation (σ) calculated. σ is then adopted as a measure of experimental uncertainty in the measurements. A comparison of the 2-D simulation and 3-D LES results follows to determine whether the 2-D results are adequate to discuss the attached boundary layer properties throughout the parameter space.

3.1. 2-D results compared to experiment

A 2-D grid resolution study was undertaken at $\alpha = 6°$, where the flow is attached and predominately 2-D. This reduces the possibility of the comparison being clouded by 3-D effects that are not captured by the 2-D models. Grid resolutions of $N_C \times N_N = 404 \times 40$ and $N_C \times N_N = 808 \times 80$ are tested. At this angle of attack the experimental lift measurement is $C_{l,exp} = 0.67 \pm 0.078$. The integrated lift calculated from both grids agree with the experimental measurements to within a 99% confidence level. Sensitivity of the results to the mesh size is evident when visualising the wake vortex structures obtained from the coarse-grid calculation. These effects are minimised in the simulation carried out on the fine-grid; consequently the fine-grid is adopted for the remainder of the study.

Simulations at additional angles of attack were carried out and it was found that up to the stall angle of $\alpha \approx 10°$, the 2-D simulations agree well with the force measurements (see Fig. 3). Post-separation, agreement with the experiments is

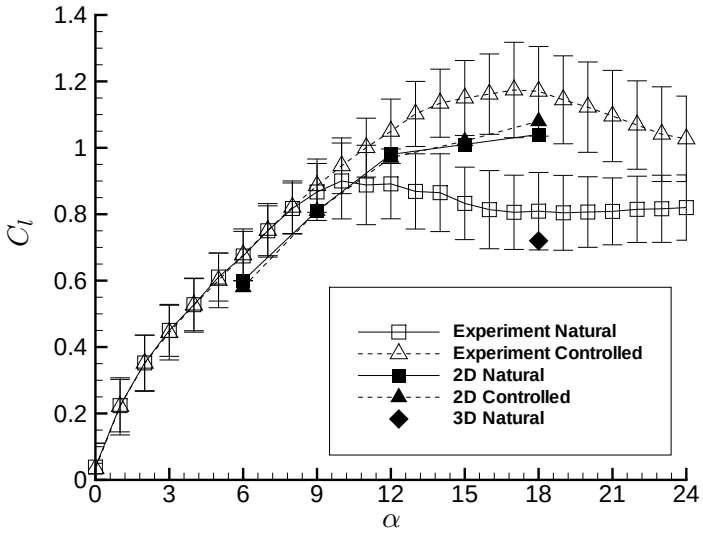

Figure 3. Lift coefficient versus α. Error bars at 99% confidence level. —□—, uncontrolled experiment; --△--, controlled experiment; —■—, uncontrolled 2-D; --▲--, controlled 2-D; ♦, uncontrolled 3-D LES. [5]

poor; this is attributed to inherent three-dimensionality in the flow, which cannot be resolved with a 2-D numerical model. A comparison of the mean streamlines in Fig. 4 also illustrates poor agreement of the 2-D simulations with the PIV measurements. The 2-D simulation exhibits a reattachment region in the uncontrolled case and a large separation bubble in the controlled case, neither of which is present in the associated PIV measurements.

3.2. 3-D LES results compared to experiment

3-D LES at $\alpha = 18°$ were carried out to investigate the significance of three dimensionality on the forces by comparing the results to the associated 2-D simulations. Only the uncontrolled case has been run to a statistically stationary state and will be presented in this paper. For this case $C_{l,exp} = 0.81 \pm 0.116$. The lift coefficient from the 3-D LES is 0.72 and within a 99% confidence level of the experimental measurements. The mean streamlines of the 3-D model in Fig. 4(e) demonstrate qualitative agreement with the PIV measurement in Fig. 4(a).

The correlation with the experimental force measurements may be improved with increased spatial resolution. In LES simulations the ratio of the maximum value within the temporally averaged eddy viscosity field ($\hat{\overline{\nu}}_{SGS}$), to the physical kinematic viscosity (ν), can be used to indicate whether the grid is fine enough for the SGS model to adequately capture the small-scale physics. In this model $\frac{\hat{\overline{\nu}}_{SGS}}{\nu} \approx 16$ in the shear regions above the airfoil, thus further refinement of the grid in these region and in the spanwise direction might be necessary.

The spanwise domain size of $1c$ used in the simulations may also limit the agreement with the experiments. In the experiment, the spanwise length is approximately $5c$, possibly allowing structures larger than $1c$ to grow in the spanwise direction. A direct

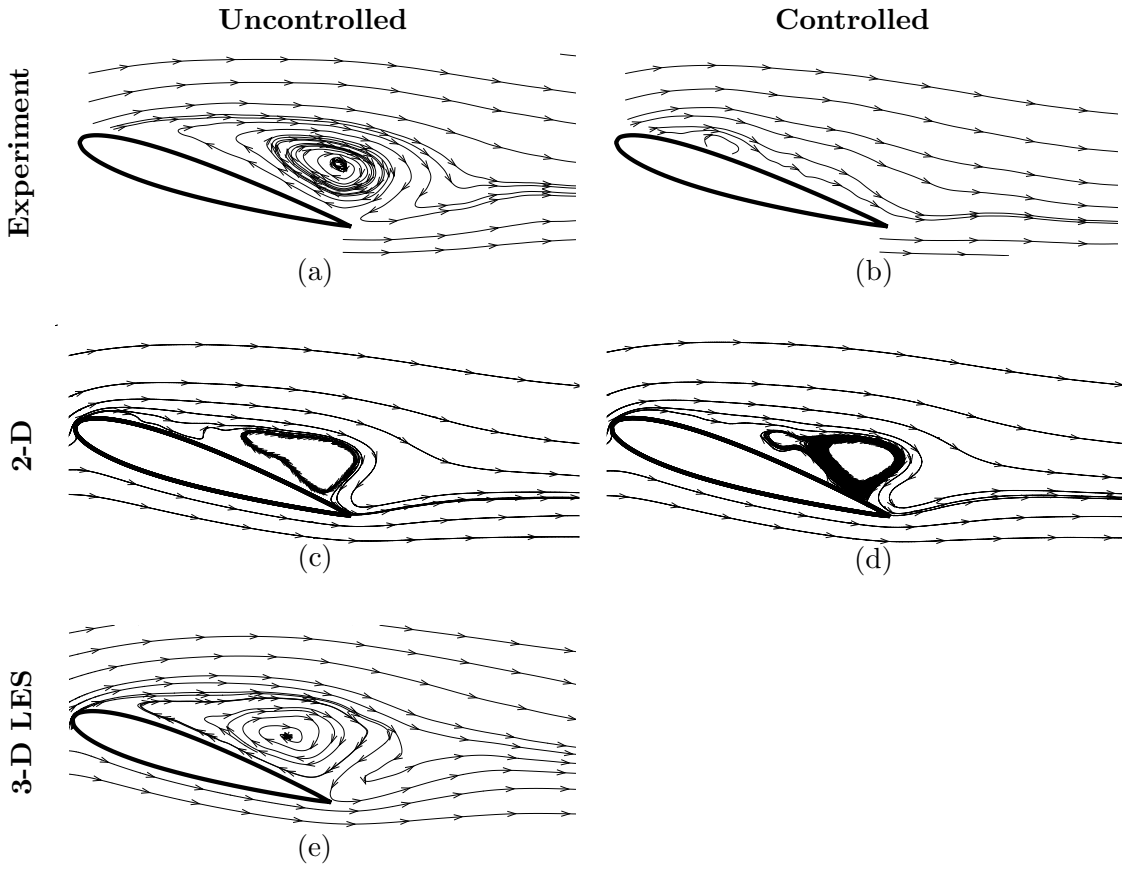

Figure 4. Mean streamlines taken at midplane of airfoil for $\alpha = 18°$. (a) uncontrolled experiment; (b) controlled experiment; (c) uncontrolled 2-D; (d) controlled 2-D; (e) uncontrolled 3-D LES. [5]

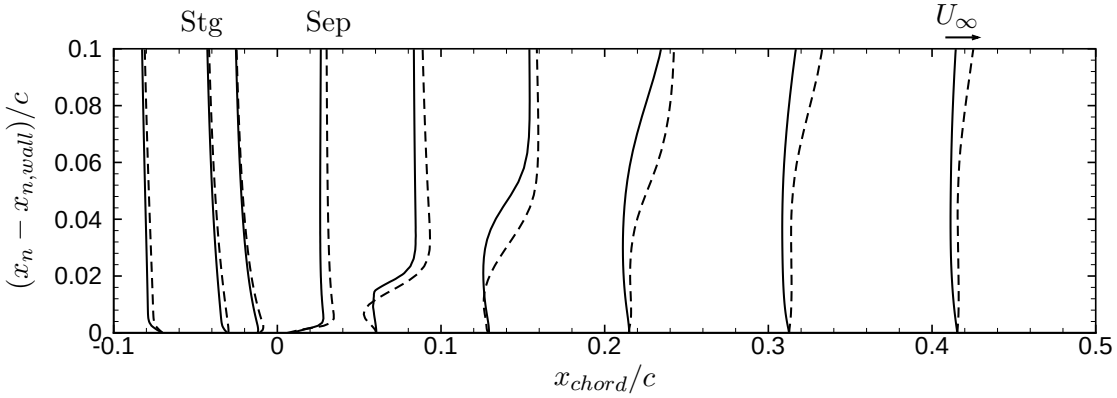

Figure 5. Comparison of the 2-D simulation and 3-D LES $\overline{u}_t$ velocity profiles of the uncontrolled case at $\alpha = 18°$. Leading edge at $x/c = 0$ with pressure side $x/c < 0$ and suction side $x/c > 0$. Stg - denoting stagnation point. Sep - denoting separation point. ----, 2-D; ——, 3-D LES. [5]

numerical simulation of a NACA 0012 airfoil with $\alpha = 20°$ and at $Re_c = 1 \times 10^4$ was undertaken by [4], where a spanwise length of $4c$ was required to resolve all spanwise scales. A mesh independency study is currently being undertaken to identify the spanwise domain size and spanwise resolution required to capture the largest scales of motion.

Initial 3-D LES simulations of the controlled case forced at $F^+ = 1.3$ had minimal impact on the flow field and hence produced negligible lift enhancement. This is inconsistent with the experimental measurements, and the discrepancy is larger than what would be expected due to possible insufficient spatial resolution. There is also some uncertainty surrounding the stated forcing frequency, however, as the ZNMF jet was generated by supplying pressure oscillations from a piston to a cylindrical chamber at the base of the cavity. The jet velocity and forcing frequency were not directly measured but inferred from the piston parameters. Structural resonances were observed in the experiments that may have modified the forcing frequency [12].

3.3. Comparison of the uncontrolled 3D-LES and 2-D simulation results

In the attached boundary layer region of the 3-D LES at $\alpha = 18°$ for the uncontrolled flow is predominately 2-D, but still in a different form of 2-D flow to that observed in the 2-D simulation. This is indicated by the spanwise rms velocity ($u_{z,rms}$) being two orders of magnitude less than the freestream, with $u_{z,rms}/U_\infty < 0.02$. The mean tangential velocity ($\overline{u}_t$) profiles are also similar in the attached region, but not identical, see Fig. 5. This is due to the 3-D structures effecting the boundary layer properties in the attached region. The 2-D results initially have a more negative $\overline{u}_t$ and then reattach at $x_{chord}/c \approx 0.21$. This explains why the integrated lift for the 2-D simulation is larger than the 3-D LES. The 2-D simulation then separates again at $x_{chord}/c \approx 0.5$ forming a separation bubble similar to the 3-D LES.

Instantaneous vortex structures further explain the reasons for the differences in the mean and rms velocity profiles. Figure 6 illustrates the vorticity contours of both the 2-D and 3-D simulations of the uncontrolled flow at $\alpha = 18°$. ω_z^Θ is the non-dimensional vorticity, given by $\omega_z^\Theta = \frac{\widehat{\omega}_t}{\Theta}$. The contour levels range between $\pm\omega_z^\Theta$ because at this contour level, the structures at the separation point are of size Θ and grow as they are convected through the domain.

Pre-separation, the flowfields are very similar. Shear layer roll up occurs in both the 2-D simulation and the 3-D LES. In the 2-D simulation distinct vortices separate from the shear layer and lift low momentum fluid up from the wall. This mechanism is responsible for the reattachment observed in the mean streamlines in Fig. 4(c). Once shed, the vortices maintain their size and strength as they are convected downstream. In the 3D-LES the vorticies are not as well defined. In this particular plane, they continue to increase in size and lose their strength until the structure transitions to freestream turbulence. The shear layer is also inclined at a higher angle and there is minimal interaction with the wall post-separation. Higher momentum fluid is therefore, not introduced to the wall and reattachment cannot occur, again consistent with the streamlines in Fig. 4(e).

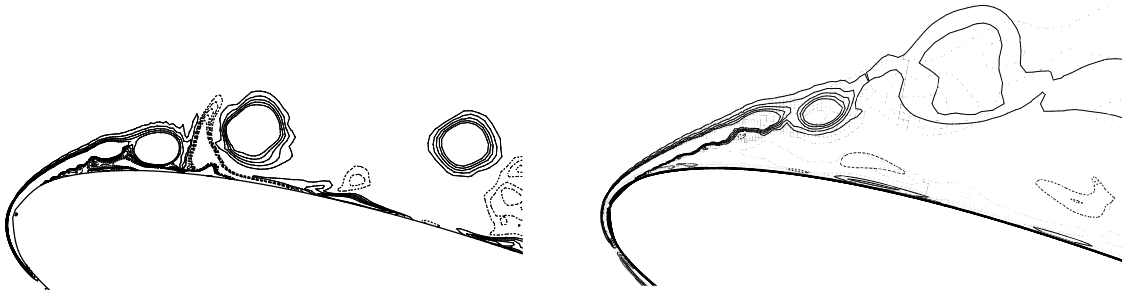

(a) (b)

Figure 6. Comparison of the 2-D simulation and 3-D LES instantaneous spanwise vorticity contours of the uncontrolled case at $\alpha = 18°$. (a) 2-D; (b) 3-D LES. 10 contour levels within $\pm\omega_z^{\Theta}$, with dashed lines indicating negative vorticity. Modified from [5].

4. Discussion on Forcing Frequency

For an airfoil where flow separates at the leading edge with no downstream reattachment, the important reattachment mechanism is the excitation of the shear layer. Forcing the shear layer at a frequency that maximises spatial amplification will initiate transition to turbulence, which will enhance mixing and draw higher momentum fluid to the wall. This will in turn induce reattachment, producing a lift enhancement. Assuming the shear layer has a parallel hyperbolic tangent profile, local stability analysis can be undertaken. Under these assumptions the frequency of the most spatially amplified wave occurs when $F^{\Theta_{SL}} = 0.032$, where $F^{\Theta_{SL}} \equiv \frac{f_{SL}\Theta_{SL}}{u_{SL}}$, Θ_{SL} is the momentum thickness of the shear layer and u_{SL} is the average velocity across the shear layer [3]. For parallel flows a local stability approach will identify the same forcing frequency for each profile.

The dimensional frequency f_{SL} is calculated at each point in the attached region for both the 2-D and 3-D uncontrolled simulations. f_{SL} is then non-dimensionalised by the cord length to identify the associated F^+_{SL}, and illustrated in Fig. 7 (a). F^+_{SL} from the 2-D simulation are offset from the 3-D case due to a larger u_{SL} in the 2-D simulation. As the airfoil flow is non-parallel, different forcing frequencies have been identified for each profile. It is assumed that the F^+_{SL} evaluated just prior to separation ($\widehat{F}^+_{SL}$) will give an indication of the frequency that will maximise spatial growth. For the 2-D simulation $\widehat{F}^+_{SL}(2D) = 9.45$ and for the 3-D simulation $\widehat{F}^+_{SL}(3D) = 7.52$. Both of these frequencies are well above the forcing frequency stated from the experiments of $F^+_{\text{exp}} = 1.3$.

The frequency space is explored with a series of 2-D simulations with $0 < F^+ < 13$ to encompass the forcing frequencies identified from the local stability analysis. Both the instantaneous spanwise vorticity contours and the velocity profiles illustrate that the 2-D and 3-D models are very similar in the attached flow region. Although the $u_{z,rms}$ profiles indicate a predominantly 2-D flow, the slight discrepancy between the $\bar{u}_t$ profiles within this attached region indicate it is a different form of 2-D flow due to the 3-D structures modifying the attached boundary layer. However, it is assumed that the 2-D results can still give an indication of how the boundary layer properties in the attached region change with forcing frequency.

The boundary layer momentum thickness Θ_{BL}, is used as a measure of attachment.

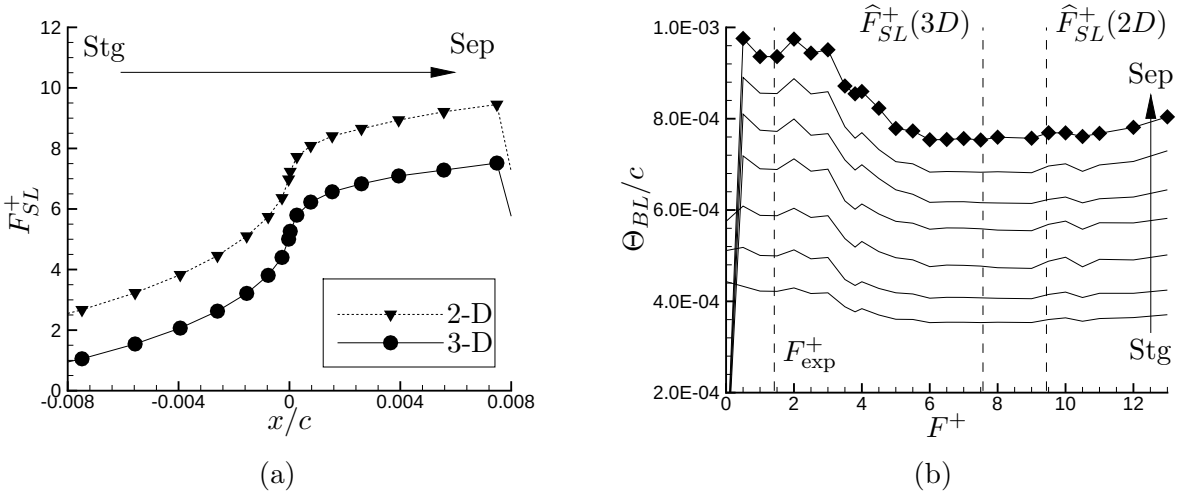

Figure 7. Determination of the frequency that will maximise lift enhancement. (a) local frequency estimated to maximise spatial growth of disturbances; (b) Θ_{BL}/c versus F^+ for various profiles between the stagnation point (Stg) and separation point (Sep). Note each diamond represents an individual 2-D simulation, and are only included on the top line for clarity.

The smaller this quantity, the steeper the velocity profile and hence less prone to separation. Figure 7 (b) illustrates the values of Θ_{BL} calculated from a series of 2-D simulations at different forcing frequencies. Θ_{BL} for each line in Fig. 7 (b) is calculated at a different position along the cord within the attached region. As the profiles shift from the stagnation point to the separation point, Θ_{BL} increases across all frequencies indicating that the velocity profiles are becoming less steep and more prone to separation. Moving in the same direction, the difference between the smallest Θ_{BL} (most attached profile) and the largest Θ_{BL}(least attached profile) also increases, producing more distinct features. The line immediately prior to separation suggests that there is a region of minimal Θ_{BL} of $5.5 < F^+ < 9.5$. Frequencies within this region effectively steepen the velocity profiles and promote reattachment. The frequencies suggested by the local stability analysis on the shear layer also lie within this region, whereas the frequency determined by the experiment does not. There are several explanations for this discrepancy. In addition to the experimental forcing frequency possibly being incorrectly stated, the numerical models may also not be dimensionally similar on the basis of fluid mechanical scales (eg: Θ), despite being dimensionally similar on the basis of chord length. As velocity profiles were not measured, it is not possible to calculate any boundary layer properties from the experimental data and directly compare the fluid mechanical scales.

5. Concluding Remarks

This paper reports on the numerical simulation of ZNMF jet lift enhancement of a NACA 0015 airfoil. The results were compared to the experimental measurements of [12]. The 3-D LES of the uncontrolled case agreed with both the PIV and force measurements, but the 3-D LES controlled case forced at $F^+ = 1.3$ exhibited minimal change in the flow field and little lift enhancement.

A forcing frequency parameter study was undertaken to which determined a range of $5.5 < F^+ < 9.5$ most effectively promoted reattachment. The frequencies suggested by the local stability analysis on the shear layer also lie within this region. However, the frequency determined by the experiment does not. This is possibly due to either the frequency in the experiment being incorrectly stated or the numerical models not being dimensionally similar on the basis of fluid mechanical scales despite being similar on the basis of cord length.
To gain further confidence in the results a mesh and domain independency study is currently being undertake to minimise any uncertainty regarding the numerical simulations.

Acknowledgements

The authors would like to acknowledge the financial contributions of the home universities. The authors also thank the Victorian Partnership for Advanced Computing (VPAC) and the Australian Partnership for Advanced Computing (APAC) for the supply of the high-performance computing resources.

References

[1] J. E. Cater and J. Soria. The evolution of round zero-net-mass-flux jets. *Journal of Fluid Mechanics*, 472:pp 167–200, 2002.

[2] M. Germano, U. Piomelli, P. Moin, and W. H. Cabot. A dynamic subgrid-scale eddy viscosity model. *Phys. Fluids A*, 3(7):1760–1765, 1991.

[3] C. Ho and P. Huerre. Perturbed free shear layers. *Annual Review of Fluid Mechanics*, 16:365–424, 1984.

[4] Y. Hoarau, M. Braza, Y. Ventikos, D. Faghani, and G. Tzabiras. Organized modes and the three-dimensional transition to turbulence in the incompressible flow around a naca0012 wing. *Journal of Fluid Mechanics*, 496:63–72, 2003.

[5] V. Kitsios, R. B. Kotapati, R. Mittal, A. Ooi, J. Soria, and D. You. Numerical study and modelling of znmf jet lift enhancement of a naca0015 airfoil. In *Proceedings of the Center for Turbulence Research Summer Program, Stanford University/NASA*, pages pp. 457–468, 2006.

[6] K. Mahesh, G. Constantinescu, and P. Moin. A numerical method for large eddy simulations in complex geometries. *J. Comput. Phys.*, 197:215 V240, 2004.

[7] H. Schlichting and K. Gersten. *Boundary layer theory*. Springer, Berlin, 8 edition, 2000.

[8] A. Seifert, T. Bachar, M. Shepshelovich, and I. Wygnanski. Oscillatory blowing: A tool to delay boundary layer separation. *AIAA Journal*, 31(11):pp. 2052–2060., 1993.

[9] B. Smith and A. Glezer. The formation and evolution of synthetic jets. *Physics of Fluids*, 10(9):2281–2297, 1998.

[10] D. Smith, M. Amitay, V. Kibens, D. Parekh, and A. Glezer. Modification of lifting body aerodynamics using synthetic jet actuators. Technical Report AIAA-98-0209, American Institute of Aeronautics and Astronautics, 1998.

[11] R. Sondergaard, R.B. Rivir, and J.P. Bons. Control of low-pressure turbine separation using vortex-generator jets. *Journal of propulsion and power*, 18:889–895, 2002.

[12] A. Tuck and J. Soria. Active flow control over a naca 0015 airfoil using a znmf jet. In *In Proceedings of the Fifteenth Australasian Fluid Mechanics Conference (CDROM)*. The University of Sydney, 2004. Paper AFMC00178.